Geochemical Perspectives Letters

Massive sulfide Zn deposits in the Proterozoic did not require euxinia

J.M. Magnall[1*], S.A. Gleeson[1,2], N. Hayward[3], A. Rocholl[1]

OPEN ACCESS

doi: 10.7185/geochemlet.2008

Abstract

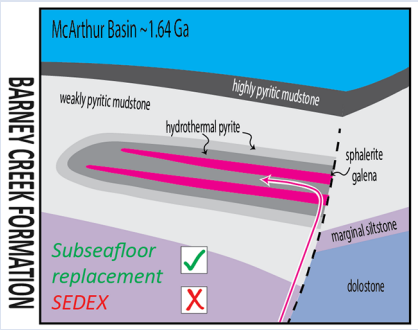

Our most important Zn resources occur within clastic-dominated (CD-type) deposits, which are located in a small number of Proterozoic and Phanerozoic sedimentary basins. The most common model for CD-type mineralisation involves sedimentary exhalative (SEDEX) processes, *i.e.* the venting of metal bearing fluids into a restricted, anoxic H_2S-bearing (euxinic) water column. In the Carpentaria Zn Province (Australia), multiple world class deposits are hosted in Proterozoic (1.6 Ga) stratigraphy, where models of the ancient sulfur cycle have also been developed. Focusing on the most recent discovery – the Teena deposit – we report bulk rock and isotopic data ($\delta^{34}S_{pyrite}$ values) that provide information on the sulfur cycle during the diagenetic and hydrothermal evolution of the Teena sub-basin. In contrast to the SEDEX model, intervals containing abundant pyrite with highly positive $\delta^{34}S$ values (>25 ‰) correspond with euxinic conditions that developed due to high organic loading (*i.e.* productivity) and not basin restriction. This basin wide feature, which can also be mistaken as a hydrothermal pyrite halo, is genetically unrelated to the subsequent hydrothermal mineralisation that formed beneath the palaeo-seafloor. The formation of CD-type deposits in the Proterozoic does not, therefore, require euxinic conditions.

Received 31 July 2019 | Accepted 27 January 2020 | Published 6 March 2020

Introduction

The Proterozoic Carpentaria Zn Province contains the largest accumulation of sediment-hosted base metals in the earth's crust (nearly 120 Mt Zn and Pb; Huston *et al.*, 2006). Deposits of the northern Carpentaria Province are of particularly broad interest, as they are hosted within one of the few low metamorphic grade marine sedimentary basins from the Proterozoic. Since the early 20th century, world class (upper 10th centile contained metal) clastic-dominated (CD-type) deposit discoveries in the Carpentaria Province have averaged one *per* 20 years (McGoldrick *et al.*, 2010). Yet with increased urbanisation and decarbonisation the global demand for Zn will continue, and some models predict a peak in Zn production within 20 years (Mohr *et al.*, 2018).

As the largest Zn reserves and resources occur in CD-type deposits, it is necessary to critically evaluate and improve existing genetic models to enhance the predictive capacity of exploration programmes. A restricted number of sedimentary basins in 2 broad time intervals (mid-Proterozoic and Palaeozoic) are known to host the largest CD-type deposits (Leach *et al.*, 2010). The most widely applied genetic model involves sedimentary exhalative (SEDEX) processes, where a sulfidic (euxinic) water column provides the *in situ* trap for hydrothermally vented metal-bearing fluids; the stratiform textures that are characteristic of CD-type deposits are then thought to result from the direct precipitation of sulfide minerals (pyrite, sphalerite, galena) from euxinic seawater (*e.g.*, Large *et al.*, 1998). Although models of Proterozoic ocean chemistry have been refined over recent decades – from the Canfield Ocean of widespread euxinia (Canfield, 1998) to more recent models in which euxinia is more spatially and temporally restricted (Poulton and Canfeld, 2011) – the SEDEX paradigm persists and mineralisation is frequently taken as *a priori* evidence that euxinic conditions were prevalent (*e.g.*, Johnston *et al.*, 2008).

In many cases, observations on the distribution and isotopic composition of pyrite provide the foundations for hydrothermal and palaeoenvironmental models (*e.g.* Lyons *et al.*, 2000; Ireland *et al.*, 2004). In this study, we focus on the most recent discovery in the Carpentaria Province – the Teena Zn-Pb deposit (Fig. S-1). Petrographic and geochemical data, collected through more than 600 m of stratigraphy, are presented for both mineralised and correlative un-mineralised samples. We demonstrate a high degree of variability in the overall abundance and isotopic composition ($\delta^{34}S$ value) of non-hydrothermal pyrite and show that euxinic conditions developed in response to high productivity during periods of

1. GFZ German Research Centre for Geosciences, 14473 Potsdam, Germany
2. Institute of Geological Sciences, Freie Universität, 74-100 Malteserstrasse, 12249 Berlin, Germany
3. Teck Australia Pty Ltd. Australia
* Corresponding author (email: joseph.magnall@gmail.com)

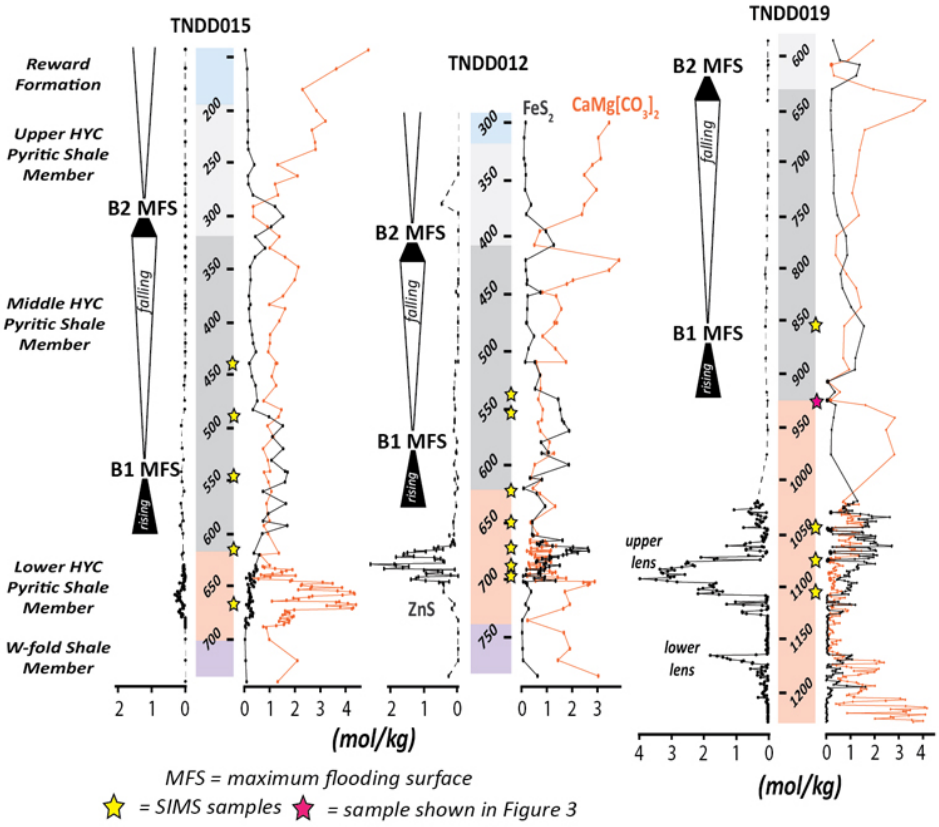

Figure 1 Chemostratigraphic sections of the Barney Creek Formation from 3 drill holes of the Teena sub-basin. Sequence stratigraphic relationships correspond with the regional framework in Kunzmann *et al.*, (2019). See Supplementary Information for further details.

high relative sea level. Contrary to the SEDEX model, hydrothermal pyrite has a much more restricted distribution and formed *via* sub-seafloor replacement processes. For exploration programmes, this means that the detectable footprint of CD-type deposits is more limited than predicted by the conventional SEDEX model.

Samples and Methods

The Teena deposit is hosted within the 1.64 Ga Barney Creek Formation (BCF) and is located approximately 8 km from the super giant McArthur River Zn-Pb deposit in correlative stratigraphy. Samples were taken from 3 drill cores that intersect the two main mineralisation lenses and the hanging wall sequence of the Teena deposit (Figs. 1 and S-2). Each sample was examined under binocular microscope, and representative sub-samples were prepared as polished thin sections for petrographic analysis. Sub-samples for isotopic microanalysis were extracted from thin section blocks using a 4 mm diameter micro-drill, and then cast into an epoxy mount for imaging and SIMS analysis. See Supplementary Information for further details.

Results

Spatial and temporal pyrite distribution. There are two main generations of pyrite, each with two sub-types: (1a) micro-crystalline (<5 µm) and occasionally framboidal pyrite, which defines discontinuous laminations (Figs. 2a and S-3a), and (1b) slightly larger (>5 µm), idiomorphic euhedral pyrite, typically formed on the margins of nodular carbonate (Fig. 2b); (2a) spherical, concentrically zoned crystals with abundant host rock inclusions (Fig. 2c), and (2b) more irregular, anhedral overgrowths, which contain interstitial sphalerite and galena mineralisation (Fig. 2d). Both sub-types of py-2 preserve As and Pb enrichments (Fig. S-4). Volumetrically minor generations of coarse grained euhedral pyrite are associated with late stage sulfide-carbonate-quartz veins (py-3).

Pyrite-1a pre-dates dolomite nodule formation (Fig. 3b inset), whereas py-1b occurs on the margins of dolomite nodules (Fig. 2b), consistent with formation during later stages of nodule growth. The pyrite associated with the sphalerite and galena is more massive, and forms anhedral overgrowths of earlier py-1 (Fig. 2d). Sphalerite does not occur within nodular dolomite, but commonly replaces nodule margins, attesting to a strictly post-nodule timing for mineralisation.

The only pyrite present throughout the stratigraphic interval is py-1a, which is highly abundant within correlative carbonaceous intervals in all 3 drill holes (Figs. 1 and S-5). All other types of pyrite are restricted either to samples containing nodular carbonate (py-1b; Fig. 2b), or to within the mineralised interval (py-2; Fig. 2c,d). In terms of a lateral pyrite halo, the overall abundance of pyrite clearly decreases within the mineralised interval (across 1.5 km from 019 > 012 > 015; Figs. 1 and S-5).

$\delta^{34}S_{pyrite}$ values. The $\delta^{34}S$ values for pyrite are shown in Figure 4. There is a strong stratigraphic control on the isotopic composition of py-1a, and highly positive $\delta^{34}S$ values are preserved in all 3 drill holes within the high pyrite abundance interval (Figs. 1 and 4). Within the mineralised intervals there is a high degree of isotopic heterogeneity within individual crystals, *i.e.* on the micro-scale. The zoned aggregates of py-2 preserve $\delta^{34}S$ values that are intermediate between the end members of py-1a, but there are no systematic trends within individual samples.

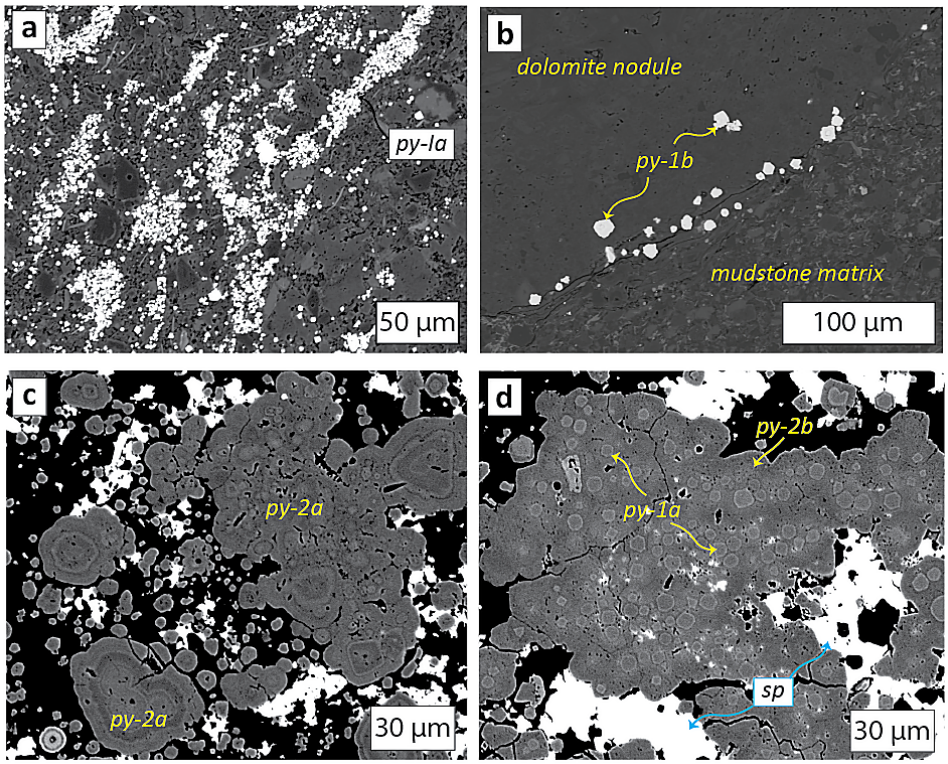

Figure 2 **(a)** Aggregates of py-1a within organic rich mudstone matrix. **(b)** Euhedral py-1b crystals within and around carbonate nodule. **(c)** Zoned aggregates of py-2a. **(d)** Aggregate of py-1a overgrown by py-2b.

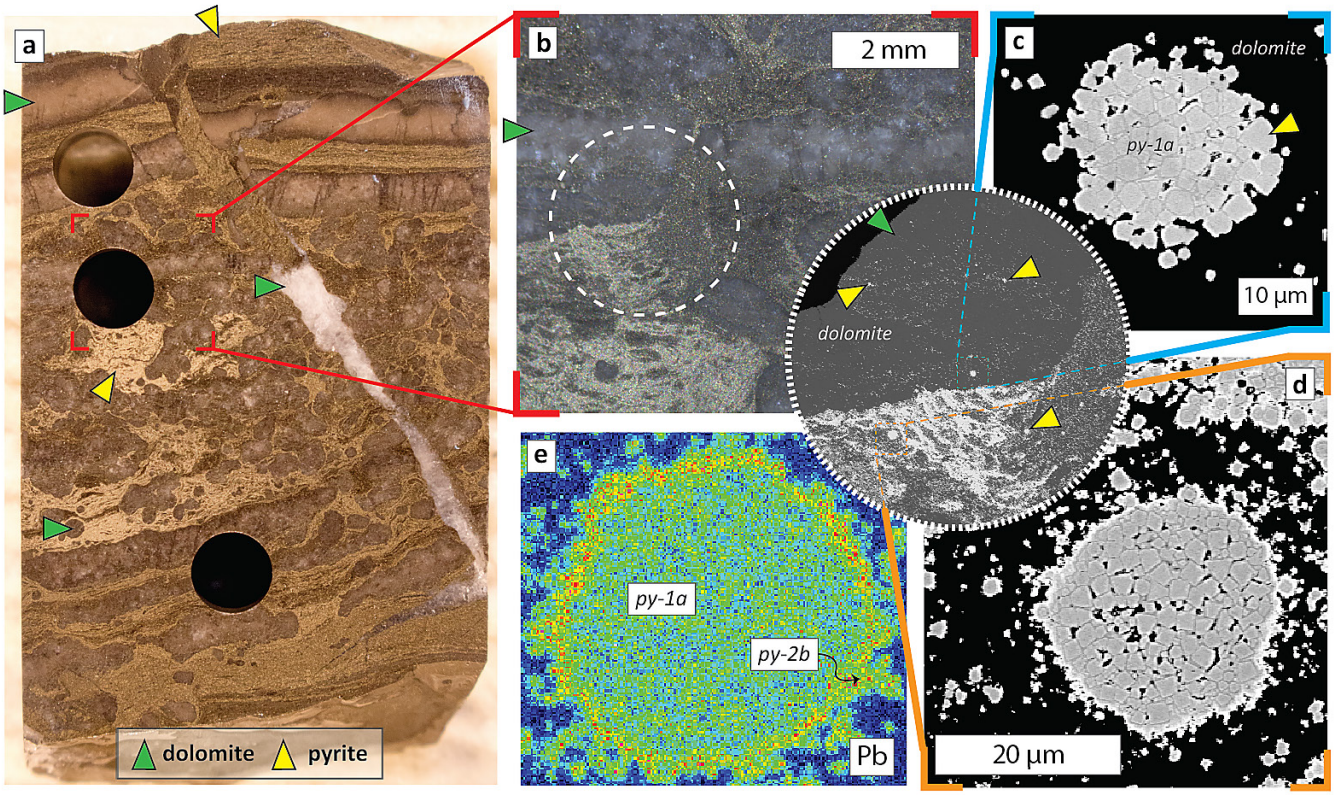

Figure 3 **(a)** Thin section block of sample selected for SIMS analysis (mineralised interval @ 925 m in 019; see Fig. 1). **(b)** Binocular photomicrograph of area selected for micro-drilling and inset showing a backscatter electron (BSE) image of the sample. Notice py-1a contained within dolomite nodule, indicating a pre-nodule origin. **(c,d)** BSE images of pyrite from the inset in **(b)**. **(e)** Electron dispersive X-ray (EDX) false colour image, showing Pb enrichment (warm colours) in the fuzzy py-2b overgrowth.

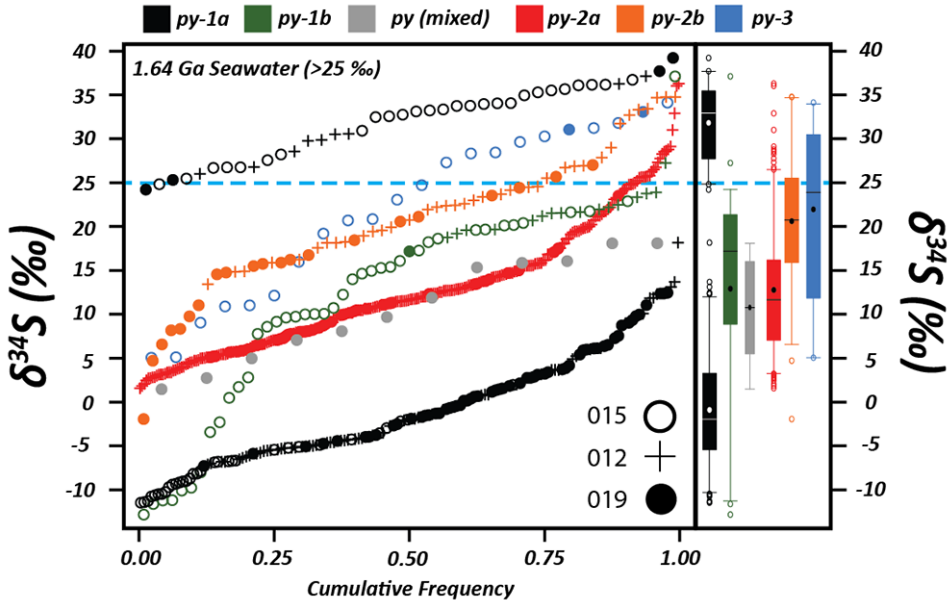

Figure 4 A cumulative frequency diagram of $\delta^{34}S$ values of all stages of the pyrite paragenesis. The sub-group of highly positive $\delta^{34}S_{py\text{-}1a}$ values is from samples from the high abundance interval. Mixed analyses where the analysis was of adjoining py-1 and 2 grains = py (mixed). The blue dashed line represents a minimum value for 1.64 Ga seawater sulfate (Li *et al.*, 2015).

Discussion

Timing and distribution of mineralisation in the Teena sub-basin. The Teena deposit shares many features (*e.g.,* stratiform sulfide textures; Fig. S-3) with the McArthur River (HYC) deposit, which is used as the type example of SEDEX mineralisation in the Carpentaria Province (Large *et al.,* 1998). In the SEDEX model, coeval formation of py-1 and sphalerite occurs within an anoxic brine pool (*e.g.,* Ireland *et al.,* 2004) and py-2 post-dates hydrothermal mineralisation (*e.g.,* Large *et al.*, 1998). These relationships are not observed in the Teena deposit as micro-scale observations show that sphalerite clearly post-dates formation of early diagenetic py-1 (*e.g.,* Fig. 2) and is interstitial to py-2 (which is also hydrothermally enriched in As and Pb; Fig. S-4).

A minimum depth constraint for the timing of mineralisation in the subsurface can be inferred from the paragenetic relationship between py-2 and nodular dolomite within the hanging wall sequence. At the top of the Lower HYC Member (925 m, TNDD019; pink star in Fig. 1), the py-1a that is overgrown by nodular dolomite has been protected from hydrothermal overgrowth (py-2b), unlike the pyrite that formed within the mudstone matrix (Fig. 3). The weak mineralisation at this higher stratigraphic level postdates the formation of nodular dolomite and represents the uppermost expression of the high grade mineralisation 200 m lower in the stratigraphy.

There is also a marked decrease in the lateral distribution of pyrite within the mineralised interval, which in TNDD015 is at levels overlapping with the un-mineralised Middle to Upper HYC Members (<0.5 mol/kg FeS_2; Fig. 1). As a result, the lateral extent of hydrothermal pyrite in the Teena sub-basin (<1.5 km; Fig. S-5) is far more restricted than the 10s of km suggested by the SEDEX model (*e.g.,* Mukherjee and Large, 2017).

Stratigraphic variability of $\delta^{34}S_{pyrite}$ values in the Teena sub-basin. The interpretation of $\delta^{34}S_{pyrite}$ values forms a common framework for both the SEDEX model and studies that focus on broader aspects of Proterozoic seawater chemistry. In either case, the development of highly positive $\delta^{34}S$ values has been linked to water mass restriction, during which microbial sulfate reduction (MSR) produced basin scale closed system Rayleigh fractionation effects (*e.g.,* Lyons *et al.,* 2000, 2006).

There is general agreement that the $\delta^{34}S$ value of 1.64 Ga seawater sulfate was >25 ‰ (Li *et al.,* 2015). Following on, the lowest $\delta^{34}S_{py\text{-}1}$ values in the Teena sub-basin represent a large offset from seawater sulfate ($\Delta^{34}S \leq 35$ ‰), typical of sulfide generated during MSR in relatively open system conditions. Pyrite associated with nodular carbonate (py-1b) is characterised by $\delta^{34}S$ values that are higher than the majority of py-1a (Fig. 4; high pyrite abundance interval excluded). The development of more positive $\delta^{34}S$ values is characteristic of sulfide generated within pore fluids during later diagenesis, either *via* MSR or sulfate reduction coupled with anaerobic oxidation of methane at the sulfate methane transition zone (*e.g.,* Borowski *et al.,* 2013; Lin *et al.,* 2016; Magnall *et al.*, 2016). In either case, the development of more positive $\delta^{34}S$ values is restricted to pore fluids and cannot be linked to water mass restriction. In contrast, the interval of high pyrite abundance preserves particularly positive $\delta^{34}S_{py\text{-}1a}$ values, which are clearly different from all other sub-types of pyrite (Fig. 4). Moreover, correlation of this interval between the 3 drill holes indicates it is not a localised effect, but a larger scale feature of the sulfur cycle in the Teena sub-basin. The development of positive $\delta^{34}S$ values on a basin scale typically occurs during pyrite formation under sulfate limited, euxinic conditions (Gomes and Hurtgen, 2015).

Water mass restriction is commonly cited as a driving mechanism for sulfate limitation in Proterozoic basins (*e.g.,* Lyons *et al.,* 2000). Nevertheless, the high pyrite abundance intervals within the BCF correspond with a marine transgression and a period of high relative sea level (Fig. 1; Kunzmann *et al.*, 2019), meaning basin restriction is unlikely to have been the primary control on sulfate limitation. Instead, we propose that sulfate limited conditions developed in a euxinic water column when a high organic carbon flux promoted MSR (Johnston *et al.,* 2010). For individual sub-basins within the McArthur Basin, rising sea level would have resulted in enhanced circulation and nutrient replenishment, following which sulfate limitation developed as a symptom of high productivity (and organic flux) rather than water mass restriction (*e.g.,* Cox *et al.,* 2016).

The evidence of sulfate limitation also poses a mass balance problem for models in which mineralisation forms from reduced sulfur derived *in situ* and entirely from seawater sulfate. For example, the maximum sulfide abundance within the MFS intervals (<1.5 mol/kg), which represents an upper limit to the reduced sulfur available under steady state conditions, is much lower than in the mineralised interval (>4 mol/kg). To satisfy the hydrothermal mass balance, therefore, requires an additional source of reduced sulfur to the system, *e.g.,* sulfur supplied by the hydrothermal fluid (Cooke *et al.,* 2000) or sour gas (Cai *et al*., 2003).

Implications. In the Teena sub-basin, the laterally extensive high abundance pyrite intervals within the hanging wall stratigraphy are unrelated to hydrothermal processes, meaning exploration strategies that focus on pyrite detection alone as an indication of prospectivity may be ineffective. Instead, pyrite formation was enhanced during periods of high biological activity that was stimulated by nutrient supply under conditions of high relative sea level. In Proterozoic basins, future researchers should avoid invoking basin wide euxinia on account of the preservation of CD-type deposits and instead focus efforts towards understanding feedbacks between sea level, nutrient supply and biological productivity (*e.g.,* Cox *et al*., 2019).

In terms of the mineral system, there is growing consensus that euxinic conditions are not a pre-requisite for the formation of CD-type deposits, either in the Proterozoic (this study) or Phanerozoic (*e.g.,* Johnson *et al.,* 2018; Magnall *et al.,* 2018). As a result, mineralisation may not necessarily occur within the most reducing lithologies and the *in situ* metal trap that is invoked by the SEDEX model should be reconsidered. Similar to hydrocarbon studies, new genetic models should be derived from more basin scale approaches that can describe subsurface hydrothermal mass transfer and metal trap dynamics. Ultimately, this will lead to a greater understanding of what restricts the distribution of CD-type deposits to a few specific basins in the geologic record and facilitate a more predictive approach to exploration.

Conclusions

The distribution of fine grained pyrite around the mid-Proterozoic Teena CD-type deposit has no relationship with hydrothermal mineralisation. Moreover, intervals of high pyrite abundance and highly positive $\delta^{34}S_{pyrite}$ values correspond with periods of high relative sea level and have no relationship with basin restriction. Mineralisation formed later and during burial diagenesis. Altogether, this means that:

(1) Evidence of sulfate limitation in Proterozoic basins is not necessarily indicative of basin restriction.

(2) Mineralisation at the Teena deposit formed during burial diagenesis, meaning CD-type deposits should not be used *a priori* as evidence of a sulfidic (euxinic) water column.

(3) Formation of the sulfide mineralisation at Teena requires an additional source of reduced sulfur, either from basinal (*e.g.,* sour gas) or hydrothermal fluids.

Acknowledgements

We acknowledge funding from the Helmholtz-Rekrutierungsinitive, thank Frederic Couffignal (GFZ) for assistance with SIMS analyses, Franzi Wilke (GFZ) for help with EPMA mapping, and Richard Stern for supplying the S0302A pyrite standard. The logistical support and permission to publish from Teck is gratefully acknowledged. Finally, we would like to thank 2 reviewers (Sam Spinks and anonymous) for their constructive comments.

Editor: Ariel Anbar

Additional Information

Supplementary Information accompanies this letter at http://www.geochemicalperspectivesletters.org/article2008.

Cite this letter as: Magnall, J.M., Gleeson, S.A., Hayward, N., Rocholl, A. (2020) Massive sulfide Zn deposits in the Proterozoic did not require euxinia. *Geochem. Persp. Let.* 13, 19–24.

References

Borowski, W.S., Rodriguez, N.M., Paull, C.K., Ussler, W. (2013) Are ^{34}S-enriched authigenic sulfide minerals a proxy for elevated methane flux and gas hydrates in the geologic record? *Marine and Petroleum Geology* 43, 381–395.

Cai, C., Worden, R.H., Bottrell, S.H., Wang, L., Yang, C. (2003) Thermochemical sulphate reduction and the generation of hydrogen sulphide and thiols (mercaptans) in Triassic carbonate reservoirs from the Sichuan Basin, China. *Chemical Geology* 202, 39–57.

Canfield, D.E. (1998) A new model for Proterozoic ocean chemistry. *Nature* 396, 450–453.

Cooke, D.R., Bull, S.W., Large, R.R., McGoldrick, P.J. (2000) The importance of oxidized brines for the formation of australian Proterozoic stratiform sediment-hosted Pb-Zn (sedex) deposits. *Economic Geology* 95, 1–18.

Cox, G.M., Jarrett, A., Edwards, D., Crockford, P.W., Halverson, G.P., Collins, A.S., Poirier, A., Li, Z.X. (2016) Basin redox and primary productivity within the Mesoproterozoic Roper Seaway. *Chemical Geology* 440, 101–114.

Cox, G.M., Sansjofre, P., Blades, M., Farkas, J., Collins, A.S. (2019) Dynamic interaction between basin redox and the biogeochemical nitrogen cycle in an unconventional Proterozoic petroleum system. *Scientific Reports* 9, 1–11.

Gomes, M.L., Hurtgen, M.T. (2015) Sulfur isotope fractionation in modern euxinic systems: Implications for paleoenvironmental reconstructions of paired sulfate-sulfide isotope records. *Geochimica et Cosmochimica Acta* 157, 39–55.

Huston, D.L., Stevens, B., Southgate, P.N., Muhling, P., Wyborn, L. (2006) Australian Zn-Pb-Ag Ore-Forming Systems: A Review and Analysis. *Economic Geology* 101, 1117–1157.

Ireland, T., Large, R.R., McGoldrick, P., Blake, M. (2004) Spatial distribution patterns of sulfur isotopes, nodular carbonate, and ore textures in the McArthur River (HYC) Zn-Pb-Ag deposit, Northern Territory, Australia. *Economic Geology* 99, 1687–1709.

Johnson, C.A., Slack, J.F., Dumoulin, J.A., Kelley, K.D., Falck, H. (2018) Sulfur isotopes of host strata for Howards Pass (Yukon-Northwest Territories) Zn-Pb deposits implicate anaerobic oxidation of methane, not basin stagnation. *Geology* 46, 619–622.

Johnston, D.T., Farquhar, J., Summons, R.E., Shen, Y., Kaufman, A.J., Masterson, A.L., Canfield, D.E. (2008) Sulfur isotope biogeochemistry of the Proterozoic McArthur Basin. *Geochimica et Cosmochimica Acta* 72, 4278–4290.

Johnston, D.T., Poulton, S.W., Dehler, C., Porter, S., Husson, J., Canfield, D.E., Knoll, A.H. (2010) An emerging picture of Neoproterozoic ocean chemistry: Insights from the Chuar Group, Grand Canyon, USA. *Earth and Planetary Science Letters* 290, 64–73.

Kunzmann, M., Schmid, S., Blaikie, T.N., Halverson, G.P. (2019) Facies analysis, sequence stratigraphy, and carbon isotope chemostratigraphy of a classic Zn-Pb host succession: The Proterozoic middle McArthur Group, McArthur Basin, Australia. *Ore Geology Reviews* 106, 150-175.

Large, R.R., Bull, S.W., Cooke, D.R., Mcgoldrick, P.J. (1998) A genetic model for the HYC deposit, Australia: Based on regional sedimentology, geochemistry, and sulfide-sediment relationships. *Economic Geology* 93, 1345–1368.

Leach, D.L., Bradley, D.C., Huston, D., Pisarevsky, S.A., Taylor, R.D., Gardoll, J. (2010) Sediment-Hosted Lead-Zinc Deposits in Earth History. *Economic Geology* 105, 593–625.

Li, C., Planavsky, N.J., Love, G.D., Reinhard, C.T., Hardisty, D., Feng, L., Bates, S.M., Huang, J., Zhang, Q., Chu, X., Lyons, T.W. (2015) Marine redox conditions in the middle Proterozoic ocean and isotopic constraints on authigenic carbonate formation: Insights from the Chuanlinggou Formation, Yanshan Basin, North China. *Geochimica et Cosmochimica Acta* 150, 90–105.

Lin, Z., Sun, X., Peckmann, J., Lu, Y., Xu, L., Strauss, H., Zhou, H., Gong, J., Lu, H., Teichert, B.M.A. (2016) How sulfate-driven anaerobic oxidation of methane affects the sulfur isotopic composition of pyrite: A SIMS study from the South China Sea. *Chemical Geology* 440, 26–41.

Lyons, T.W., Luepke, J.J., Schreiber, M.E., Zieg, G.A. (2000) Sulfur geochemical constraints on Mesoproterozoic restricted marine deposition: Lower Belt Supergroup, northwestern United States. *Geochimica et Cosmochimica Acta* 64, 427–437.

Lyons, T.W., Gellatly, A.M., McGoldrick, P.J., Kah, L.C. (2006) Proterozoic sedimentary exhalative (SEDEX) deposits and links to evolving global ocean chemistry. *Geological Society of America Memoirs* 198, 169–184.

Magnall, J.M., Gleeson, S.A., Stern, R.A., Newton, R.J., Poulton, S.W., Paradis, S. (2016) Open system sulphate reduction in a diagenetic environment - isotopic analysis of barite ($\delta^{34}S$ and $\delta^{18}O$) and pyrite ($\delta^{34}S$) from the Tom and Jason Late Devonian Zn-Pb-Ba deposits, Selwyn Basin, Canada. *Geochimica et Cosmochimica Acta* 180, 146–163.

Magnall, J.M., Gleeson, S.A., Poulton, S.W., Gordon, G.W., Paradis, S. (2018) Links between seawater paleoredox and the formation of sediment-hosted massive sulphide (SHMS) deposits – Fe speciation and Mo isotope constraints from Late Devonian mudstones. *Chemical Geology* 490, 45–60.

McGoldrick, P., Winefield, P., Bull, S., Selley, D., Scott, R. (2010) Sequences, Synsedimentary Structures, and Sub-Basins: the Where and When of SEDEX Zinc Systems in the Southern McArthur Basin, Australia. *Economic Geology Special Publication*, 367–389.

Mohr, S., Giurco, D., Retamal, M., Mason, L., Mudd, G. (2018) Global Projection of Lead-Zinc Supply from Known Resources. *Resources* 7, 1–15.

Mukherjee, I., Large, R. (2017) Application of pyrite trace element chemistry to exploration for SEDEX style Zn-Pb deposits: McArthur Basin, Northern Territory, Australia. *Ore Geology Reviews* 81, 1249–1270.

Poulton, S.W., Canfeld, D.E. (2011) Ferruginous conditions: A dominant feature of the ocean through Earth's history. *Elements* 7, 107–112.

Geochemical Perspectives Letters

Massive sulfide Zn deposits in the Proterozoic did not require euxinia

J.M. Magnall, S.A. Gleeson, N. Hayward, A. Rocholl

Supplementary Information

The Supplementary Information includes:

- Geological Setting
- Methodology
- Table S-1
- Figures S-1 to S-5
- Supplementary Information References

Geological Setting

The Carpentaria Zn Province is located in northern Australia (Fig. S-1a). Clastic-dominant (CD-type) Zn-Pb sulfide deposits are hosted primarily within carbonaceous mudstones of Proterozoic age in the Mt Isa – McArthur Basin. The Teena and McArthur River deposits occur within the Barney Creek Formation (BCF), which represents the peak transgressive phase of the River Supersequence depositional cycle (Page *et al*., 2000). The age of the Barney Creek Formation is constrained by U-Pb geochronology of zircons from the underlying Teena Dolostone (1639 ± 6 Ma) and the overlying Lynott Formation (1636 ± 4 Ma; Page *et al*., 2000). Zircons from volcaniclastic units within central BCF provide constraints of 1638 ±7 Ma, 1639 ± 3 Ma, and 1640 ± 3 Ma (Page and Sweet, 1998).

The sedimentary units of the BCF are regionally subdivided into the lower W-Fold Shale and overlying HYC Pyritic Shale members (Jackson *et al*., 1987; Pietsch *et al*., 1991). In the Teena sub-basin, the HYC Pyritic Shale members are sub-divided into the Lower, Middle and Upper members. At the McArthur River deposit, the sulfide mineralisation is located within the Lower HYC unit, which comprises variably dolomitic, silty carbonaceous mudstones, and is considered to be the deepest-water facies (Ireland *et al*., 2004; McGoldrick *et al*., 2010). The Teena deposit is also hosted within correlative stratigraphy of the Lower HYC, approximately 8 km away (see Fig. S-1b).

Both the W-fold Shale and HYC units preserve exhibit wedge-shaped geometries with abrupt thickening proximal to syndepositional growth faults (*e.g.*, McGoldrick *et al*., 2010; Kunzmann *et al*. 2019). Pronounced lateral lithofacies variations and local unconformities that indicate a change in depositional setting from a carbonate-dominated stable shallow marine platform, to a compartmentalized basin with numerous sub-basins and local paleo-highs associated with the onset of syndepositional extensional faulting and a marine transgression (McGoldrick *et al*., 2010). Some of the thickest parts of the Barney Creek depositional cycle occur within the Hot Spring-Emu sub-basin (Fig. S-1b), which hosts the McArthur River deposit in the northeast corner, and the

Teena deposit further west along the Bald Hills Fault.

There are 2 maximum flooding surfaces (MFS) within the Barney Creek Formation, recognisable from the high pyrite and organic carbon content, and which can be correlated across the entire McArthur Basin (Kunzmann *et al*., 2019). In the Teena sub-basin, the MFS intervals overly sequences of lesser pyritic mudstones that also contain a peak in carbonate (Fig. 1). We interpret this carbonate peak as being associated with reduced sedimentation rates during marine transgressions, thereby leading to the increased residence time of individual sedimentary packages within early diagenesis and corresponding higher levels of carbonate cementation (Taylor *et al*., 1995).

Following the development of their sequence stratigraphic framework, Kunzmann *et al*. (2019) suggested that sulfide mineralisation (with McArthur River used as an example) is likely associated with the development of these MFS intervals, owing to the high levels of sulfide and organic carbon. Notably, the sulfide mineralisation in the Teena sub-basin is actually located beneath the B1 MFS interval, and not within an obvious MFS interval. For example, there is a strong lateral decrease in pyrite abundance within the mineralised horizon, which for samples from TNDD015 drops to the levels observed within the Middle and Upper HYC units (termed Undifferentiated Barney Creek by Kunzmann *et al*., 2019). We would argue, therefore, that the mineralisation in the Teena sub-basin does not coincide with a MFS interval, as is frequently suggested for these deposits.

Methodology

A total of 3 mounts were prepared (one for each drill-hole), containing sub-sample pucks from 17 samples and multiple grains of the S0302A standard ($\delta^{34}S$ = 0.2 +/- 0.2 ‰; Magnall *et al*., 2016). Each mount was coated with Au and imaged using scanning electron microscopy (SEM; GFZ Potsdam). Sulfur isotope analyses were produced using a Cameca 1280-HR Secondary Ion Mass Spectrometer (SIMS) at the Helmholtz Zentrum (Potsdam). The primary beam (20 KeV $^{133}C^+$) was focused to a beam diameter of 5 µm. Simultaneous analysis of the isotopes of interest (^{32}S and ^{34}S) was conducted following the extraction of negatively charged secondary ions into Faraday Cups. The accuracy and precision of the data were monitored through the analysis of the standard, in duplicate, every 10 analyses. Time-dependent instrumental mass fractionation was determined for each analytical session and corrected for. Final uncertainties were between 0.2 and 1.0 ‰ (2σ) for each analysis.

Sulfide abundances were calculated on the basis of whole rock geochemical analyses of drill-core samples (Magnall *et al*., in prep.). Quarter core samples were sent for major element and assay (Cu, Pb, Zn) analysis with Bureau Veritas (Mt Isa) using oxidative fusion followed by XRF analysis.

As the only sulfide phases present are pyrite (FeS_2), sphalerite (ZnS) and galena (PbS), pyrite (mol/kg) was calculated as S_pyrite(mol/kg) = S_mol/kg – (Zn_mol/kg + Pb_mol/kg). A 1:1 correlation between Ca and Mg means that Ca_mol/kg provides a reliable approximation of total dolomite $CaMg[CO_3]_2$.

Supplementary Tables

Table S-1 Sulfur isotope data for SIMS analyses of pyrite at the Teena deposit. Data are described by lithological unit, paragenesis, and the dominant mineral assemblage within the individual sample puck that was extracted from the hand sample (*e.g.,* mudstone matrix, dolomite nodule *etc.*).

Table S-1 is available for download at http://www.geochemicalperspectivesletters.org/article2008.

Supplementary Figures

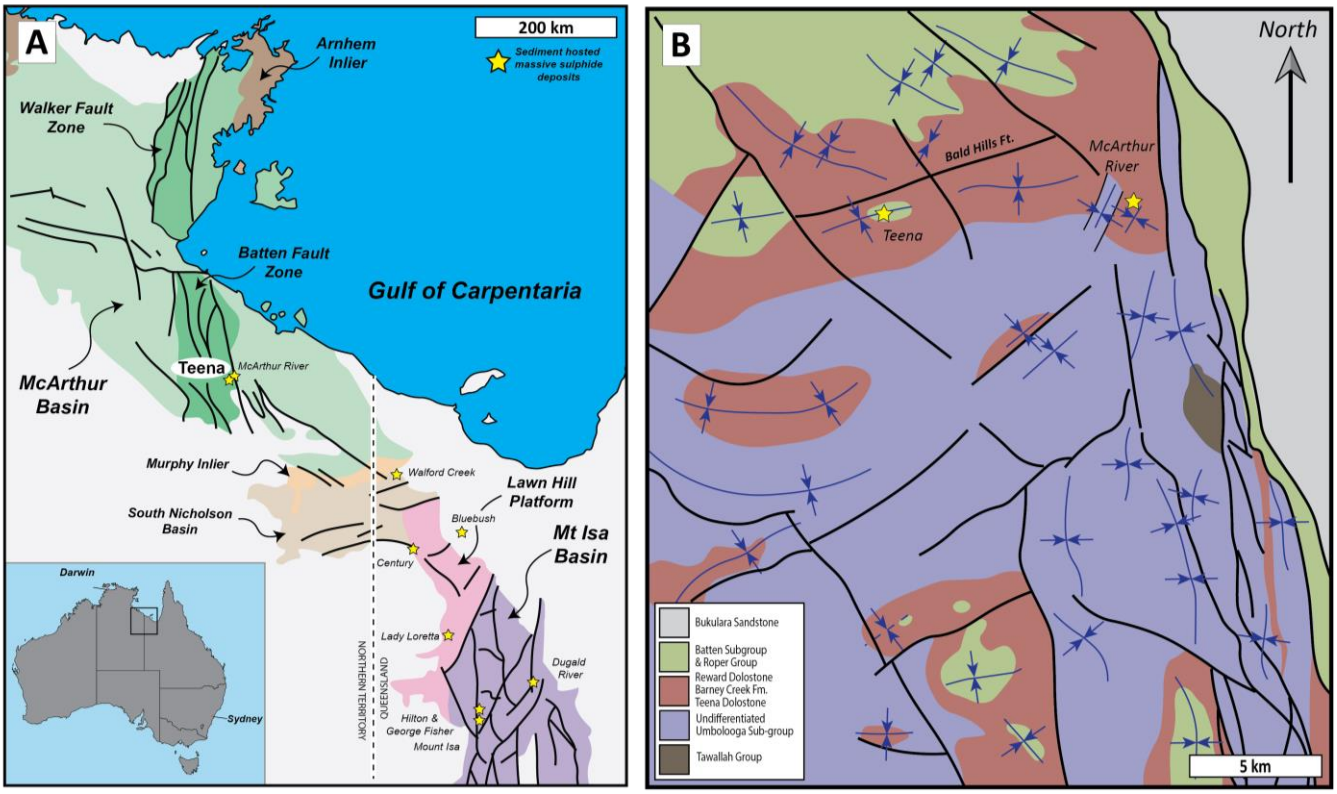

Figure S-1 **(a)** Map showing the geographical extent of the McArthur – Mt Isa basin and the locations of CD-type deposits (denoted by stars). **(b)** Sub-basins within the Emu-Hot Springs sub-basin. Both figures modified from McGoldrick *et al*. (2010).

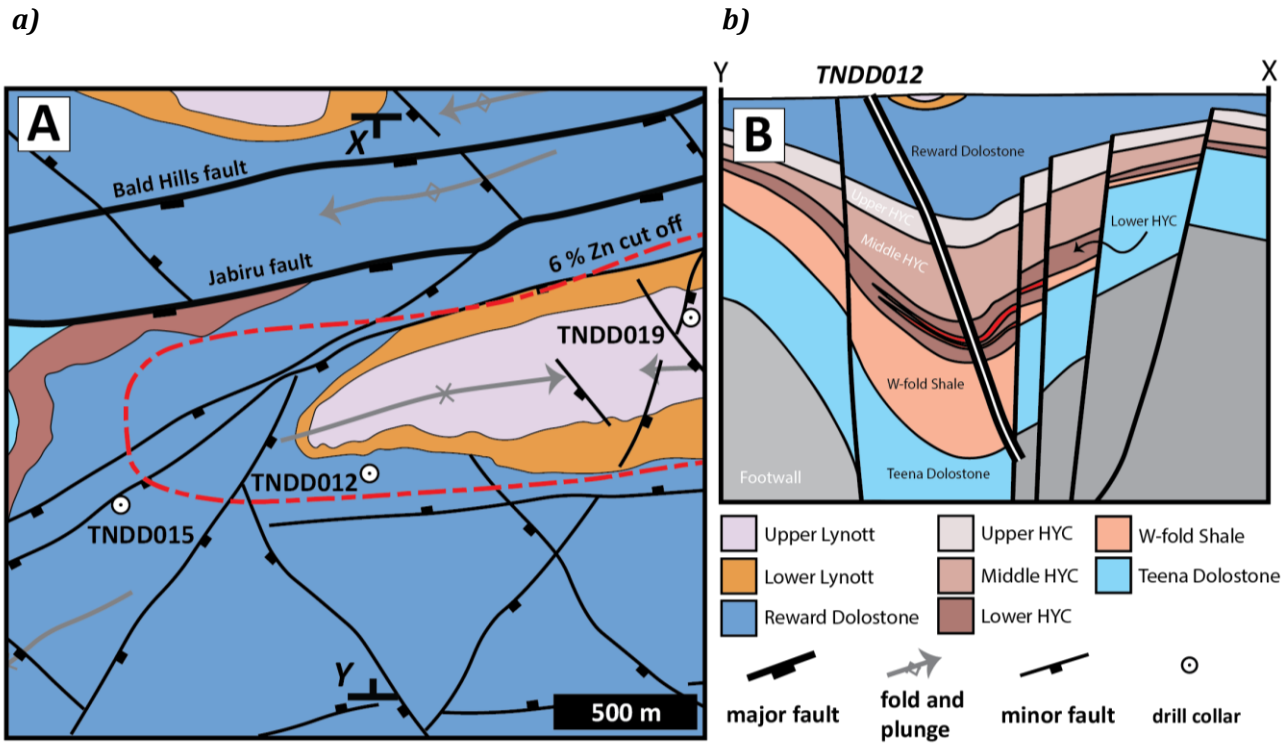

Figure S-2 **(a)** interpreted plan view geological map of the Teena sub-basin showing the main lithologies, geological structures (faults, folds) and drill-hole collars. **(b)** Schematic cross-section through the Teena sub-basin. Sulfide mineralistion occurs within the Lower HYC unit, and is coloured red.

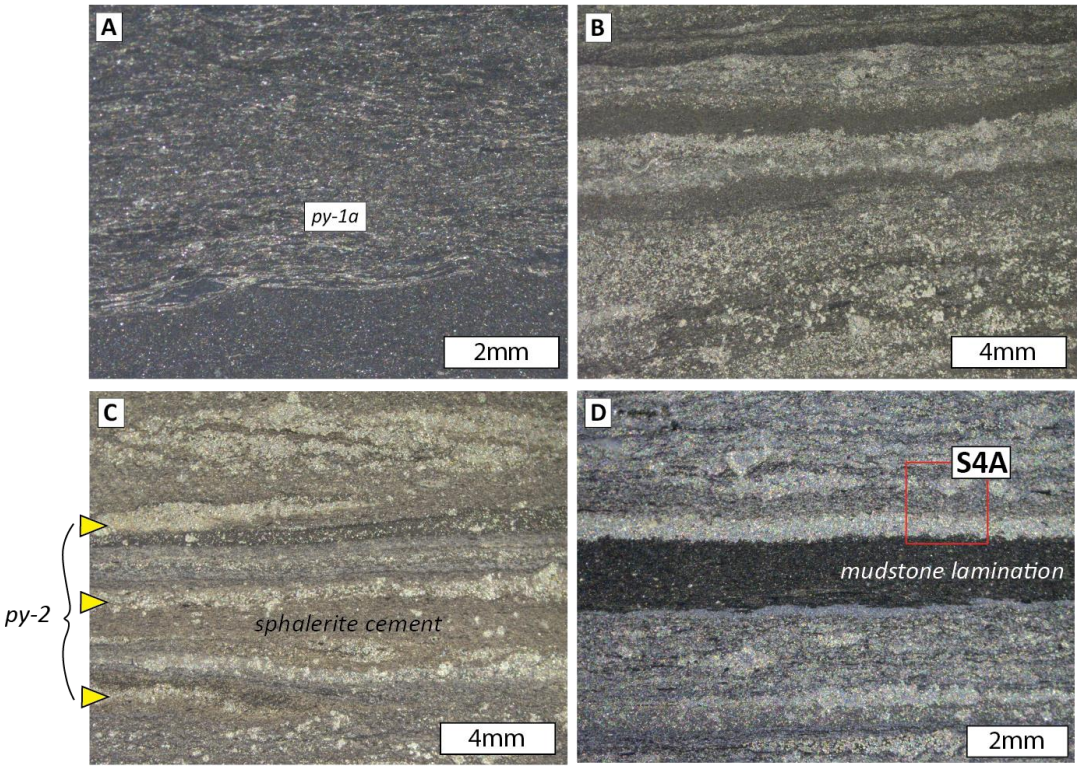

Figure S-3 Binocular microscope photographs of pre-ore and ore stage sulfide mineralisation from drill-core hand samples. **(a)** Discontinuous wispy aggregates of Py-1a within a carbonaceous mudstone sample from the maximum flooding surface high pyrite abundance interval in the upper HYC. **(b)** Stratiform aggregates of Py-2 with weak sphalerite cement mineralisation in the lower HYC mineralised interval. **(c)** Strong sphalerite cement mineralisation in the lower HYC mineralised interval. **(d)** Sharp contact between un-mineralised mudstone lamination and sphalerite and galena cement mineralisation within the lower HYC mineralised interval.

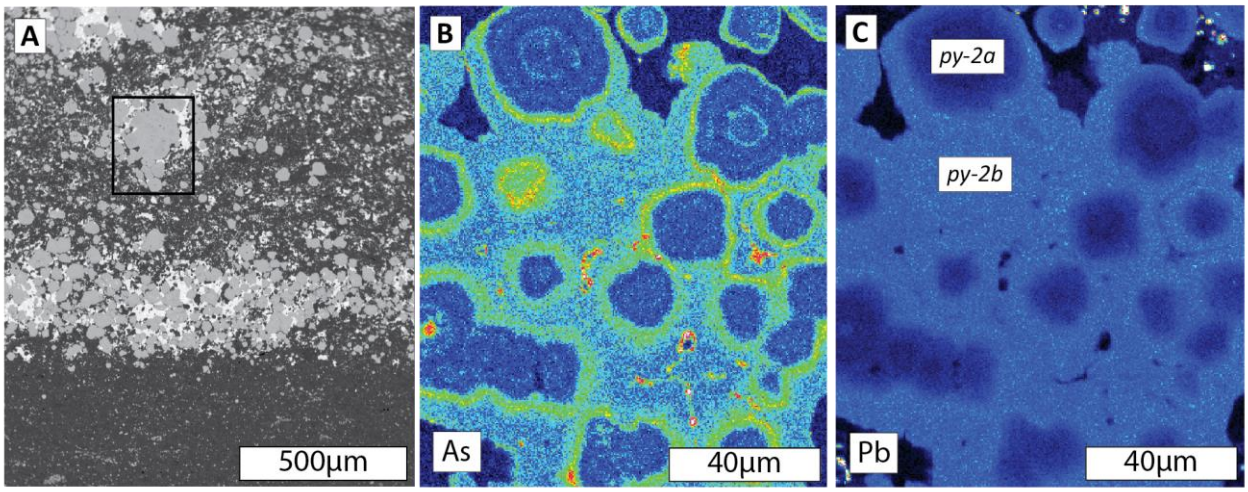

Figure S-4 **(a)** Backscatter electron (BSE) image of the interface between the mudstone lamination in **Figure S-2d** and ore stage sulfide cement mineralisation within the overlying stratiform pyrite. **(b)** Energy dispersive X-ray (EDX) mapping of As distribution within a zoned aggregate of Py-2. **(c)** EDX mapping of Pb distribution within a zoned aggregate of Py-2.

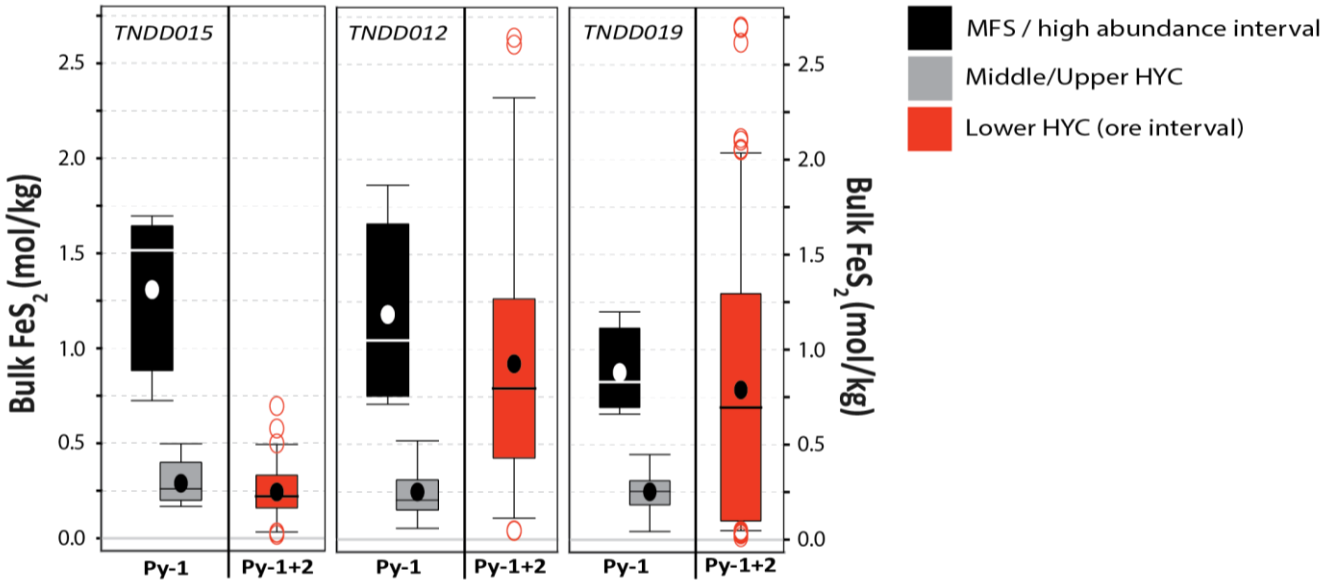

Figure S-5 Box and whisker plots for pyrite abundance (mol/kg; calculated from bulk rock) through the Lower and Middle HYC units of the Barney Creek Formation. The mineralisation is located within the Lower HYC unit, and there is clear lateral zonation in pyrite abundance from drill hole TNDD015 (un-mineralised) to TNDD012 (moderately mineralised) to TNDD019 (strongly mineralised). The high abundance pyrite interval located within the maximum flooding surface (MFS; black) has been separated from the rest of the Middle HYC (grey). Whereas the Middle and Upper HYC units contain primarily Py-1, the Lower HYC mineralised interval contains a mixture of Py-1 and Py-2 (predominantly Py-2 within TNDD019 and TNDD012).

Supplementary Information References

Ireland, T., Large, R.R., McGoldrick, P., Blake, M. (2004) Spatial Distribution Patterns of Sulfur Isotopes, Nodular Carbonate, and Ore Textures in the McArthur River (HYC) Zn-Pb-Ag Deposit, Northern Territory, Australia. *Economic Geology* 99, 1687–1709.

Jackson, M.J., Muir, M.D., Plumb, K.A., Jackson M.J. (1987) Geology of the southern McArthur Basin, Northern Territory (Australia). *Bulletin - Bureau of Mineral Resources, Geology & Geophysics, Australia*, 220.

Kunzmann, M., Schmid, S., Blaikie, T.N., Halverson, G.P. (2019) Facies analysis, sequence stratigraphy, and carbon isotope chemostratigraphy of a classic Zn-Pb host succession: The Proterozoic middle McArthur Group, McArthur Basin, Australia. *Ore Geology Reviews* 106, 150-175.

Magnall, J.M., Gleeson, S.A., Stern, R.A., Newton, R.J., Poulton, S.W., Paradis, S. (2016) Open system sulphate reduction in a diagenetic environment - Isotopic analysis of barite ($\delta^{34}S$ and $\delta^{18}O$) and pyrite ($\delta^{34}S$) from the Tom and Jason Late Devonian Zn-Pb-Ba deposits, Selwyn Basin, Canada. *Geochimica Cosmochimica Acta* 180, 146–163.

McGoldrick, P., Winefield, P., Bull, S., Selley, D., Scott, R. (2010) Sequences, Synsedimentary Structures, and Sub-Basins: the Where and When of SEDEX Zinc Systems in the Southern McArthur Basin, Australia. *Economic Geology Special Publication* 15, 367–389.

Page, R.W., Sweet, I.P. (1998) Geochronology of basin phases in the western Mt Isa Inlier, and correlation with the McArthur Basin. *Australian Journal of Earth Sciences* 45, 219-232.

Page, R.W., Jackson, M.J., Krassay, A.A. (2000) Constraining sequence stratigraphy in north Australian basins: SHRIMP U-Pb zircon geochronology between Mt Isa and McArthur River. *Australian Journal of Earth Sciences* 47, 431–459.

Pietsch, B.A., Rawlings, D.J., Creaser, P.M., Kruse, P.D., Ahmad, M., Ferenczi, P.A., Findhammer, T.L.R. (1991) 1:250,000 Geological Map Series Explanatory Notes, Bauhinia Downs SE53-3.

Taylor, K.G., Gawthorpe, R.L., Van Wagoner, J.C. (1995) Stratigraphic control on laterally persistent cementation, Book Cliffs, Utah. *Journal of the Geological Society London* 152, 225–228.